Chaos and fractals in geodesic motions around a nonrotating black hole with halos

Alessandro P. S. de Moura*
Instituto de Física Gleb Wataghin, UNICAMP, 13083-970 Campinas Sao Paulo, Brazil

Patricio S. Letelier†
Instituto de Matemática, Estatística e Ciência da Computação, Departamento de Matemática Aplicada, UNICAMP, 13083-9790 Campinas Sao Paulo, Brazil

(Received 27 August 1999; revised manuscript received 22 February 2000)

We study the escape dynamics of test particles in general-relativistic gravitational fields generated by core-shell models, which are used in astrophysics as idealized models to observed mass distributions, such as the interior of galaxies. As a general-relativistic core-halo system, we use exact axisymmetric static solutions of Einstein's field equations which represent the superposition of a central Schwarzschild black hole (the core) and multipolar fields from external masses (the halo). We are particularly interested in the occurrence of chaos in the escape, which is characterized by a great sensitivity of the choice of escape by a test particle to initial conditions. The motion of both material particles and zero rest mass particles is considered. Chaos is quantified by the fractal dimension of the boundary between the basins of the different escapes. We find chaos in the motion of both material particles and null geodesics, but its intensity depends strongly on the halo. We have found for all the cases we have considered that massless particles are less chaotic than massive particles.

PACS number(s): 05.45.Df, 95.10.Fh, 95.30.Sf, 05.45.Pq

I. INTRODUCTION

Core-shell gravitational systems play an important role in astrophysics, because they can be used as approximations to observed astronomical distributions of masses. These systems are characterized by a central massive core (possibly a black hole) and a surrounding halo of matter. The space between the core and the halo is assumed to be empty, and the gravitational field there satisfies the vacuum field equations. In real systems the assumption that the region between the core and the halo is empty is clearly not satisfied, but it may be approximately valid in some cases.

In Newtonian gravitation, a general way of treating the field of the halo is by means of a multipole expansion. Each multipole term is a solution of Laplace's equation, which increase with distance, contrary to the more usual decreasing multipoles. The field of a general halo can always be written as a linear superposition of such multipole terms. In general relativity, the situation is more complicated, because Einstein's field equations are not linear. However, in the particular case of axisymmetric (and static) vacuum fields, a general solution of the field equations is known, and this solution is parametrized by a certain metric function that is related in a simple way to the Newtonian gravitational field in the limit of weak fields, and it can be used to perform a multipole expansion. Although such expansion is by no means unique, and its relationship with the Newtonian expansion is far from straightforward, it is still valuable and can be used to describe the general-relativistic gravitational field of a general halo.

This article is concerned with the motion of test particles (both massive particles and light will be considered) in a core-shell system in the region between the core (which we assume to be a nonrotating black hole) and the halo, whose gravitational field in this region is described by a multipole sum, in which we keep terms of up to the third order (octopole). The treatment is fully relativistic, using exact solutions of Einstein's equations that describe the gravitational (vacuum) field due to the superposition of the fields of a Schwarzschild black hole and the various multipole components of the halo; in some cases we also use the corresponding Newtonian field to compare the results. The motion of test particles in the core-halo field may depend on several parameters: the energy, the angular momentum, the multipole strengths, etc. Depending on the values of these parameters, the motion may be either bounded or unbounded. Bounded motion means that the particle is restricted to a finite volume of phase space; unboundedness means that a particle has access to an infinite phase-space volume. In this paper, we are interested in the escape properties of these systems. If a system has two or more physically well-defined escapes for a given set of parameters of the metric (for instance, regions where a particle runs away to infinity, or where it falls into an event horizon), then the escape it chooses depends on the initial conditions; when the basins of escape have a fractal structure, we have a well-defined kind of chaos, and the corresponding fractal dimension gives a good quantitative characterization of chaos, besides having a simple physical interpretation as a measure of the sensitivity to initial conditions (see Sec. III). Since the fractal nature of the boundary between the basins of escape is a topological feature, it is independent of the choice of the space-time coordinates; this assures the meaningfulness of this characterization for general relativity.

The study of chaos in dynamical systems with unbounded orbits is relatively recent [1]. The characterization of chaos for this class of problems is different from that used for bounded Hamiltonian dynamics, which is based upon the

*Present address: Institute for Plasma Research, A.V. Williams Building, University of Maryland, College Park, MD 20742-3511. Electronic address: sandro@ifi.unicamp.br

†Electronic address: letelier@ime.unicamp.br

destruction of Kolmogorov-Arnol'd-Moser (KAM) tori. One of the most important situations with unbounded motion is that of the escape of particles from a certain region; this problem is closely related to scattering, the difference between the two being essentially the choice of the initial conditions. Escapes have been studied for several systems: two-dimensional autonomous Hamiltonian systems [2–4], nonlinear oscillations [5,6], two-dimensional conservative mappings [7], chaotic cosmology [8,9], and multiple-black-hole space-times [10–12] are only a few examples.

This paper is organized as follows: in Sec. II we review the general vacuum static axisymmetric metric and some of its properties; and in Sec. III we define the box-counting dimension and discuss its physical significance. In Sec. IV, we investigate the basins of escape in the motion of material particles for some choices of static axisymmetric metrics, and show numerically the existence of chaos; the axial and temporal symmetries of the space-time allow us to define a two-dimensional ''effective potential,'' which as in the Newtonian case determines the regions in space that are accessible to the particle, thereby making the analysis of the relativistic system analogous to that of the Newtonian systems in many ways. In Sec. V, we show that null geodesics are regular (nonchaotic) in the field of a dipolar halo (plus the black hole), but chaos arises if we add multipole moments of higher order to the halo; and in Sec. VI we summarize our results and draw some conclusions.

II. THE WEYL METRIC

Many astrophysical systems have axial symmetry, and their mass distribution can often be approximated by a static configuration. Throughout this article, we consider only axisymmetric static gravitational fields, and use the Weyl metric to describe a general static axisymmetric space-time [13]:

$$ds^2=e^{2\psi}dt^2-e^{-2\psi}[e^{2\gamma}(dr^2+dz^2)+r^2d\phi^2], \tag{1}$$

where r and z are the radial and axial coordinates, and ϕ is the angle about the z axis, which is the axial symmetry axis. Throughout this article, we will use units such that $c=1$ and $m=1$, where m is the mass of the central black hole (1). ψ and γ are functions of r and z only. In these coordinates, the vacuum Einstein equations reduce to

$$\frac{\partial^2\psi}{\partial r^2}+\frac{1}{r}\frac{\partial\psi}{\partial r}+\frac{\partial^2\psi}{\partial z^2}=0, \tag{2}$$

$$d\gamma=r\left[\left(\frac{\partial\psi}{\partial r}\right)^2-\left(\frac{\partial\psi}{\partial z}\right)^2\right]dr+2r\frac{\partial\psi}{\partial r}\frac{\partial\psi}{\partial z}dz. \tag{3}$$

The first expression is just Laplace's equation in cylindrical coordinates; the second equation defines γ, once ψ is found. From Eq. (2) and the form of the metric (1) it is clear that in the weak-field limit Ψ can be identified as the Newtonian scalar gravitational field.

The metric (1) is independent of the time t and of the symmetry angle ϕ. From this we obtain the two constants of motion $\hat{E}$ (energy) and $\hat{L}_z$ (projection of the angular momentum on the symmetry axis), that are conserved along the trajectories of test particles in the metric (1). They are given by

$$\hat{E}\equiv p_t=g_{tt}\dot{t}, \tag{4}$$

$$\hat{L}_z\equiv p_\phi=g_{\phi\phi}\dot{\phi}, \tag{5}$$

where the overdot denotes differentiation with respect to the proper time in the case of a massive test particle, or an affine parameter, in the case of particles with zero rest mass. The only independent dynamical variables are thus r and z and their momenta p_r and p_z: the time evolution of t and ϕ is given by the quadratures above. This means that the dynamical system corresponding to the motion of test particles in the Weyl metric has only two degrees of freedom.

Besides the energy and the z component of the angular momentum, there is another quantity that is conserved along the trajectory of a test particle, namely, its rest mass. This conserved quantity is given by

$$g^{\mu\nu}p_\mu p_\nu=\hat{E}^2g^{tt}+\hat{L}_z^2g^{\phi\phi}+f(\dot{r}^2+\dot{z}^2)=m_0^2, \tag{6}$$

where $f=-g_{rr}=-g_{zz}=e^{2(\psi-\gamma)}$ and m_0 is the rest mass of the test particle, which must satisfy $m_0\ll 1$. Dividing both sides by m_0 (if $m_0\neq 0$), we rewrite the above equation in a more convenient form:

$$E^2g^{tt}+L_z^2g^{\phi\phi}+f(\dot{r}^2+\dot{z}^2)=\delta, \tag{7}$$

where $E=\hat{E}/m_0$ is the test particle's energy per mass, $L_z=\hat{L}_z/m_0$ is the z component of the angular momentum per mass, and the overdot now means differentiation with respect to the new affine parameter obtained from the previous one by multiplication by m_0. $\delta=1$ for massive particles, and $\delta=0$ for particles with zero rest mass. The conservation equations for the scaled quantities E and L_z are

$$E=g_{tt}\dot{t}, \tag{8}$$

$$L_z=g_{\phi\phi}\dot{\phi}. \tag{9}$$

Remember that the differentiation is performed with the scaled affine parameter.

The equations of motion for the test particles are

$$\ddot{x}^\mu+\Gamma^\mu_{\alpha\beta}\dot{x}^\alpha\dot{x}^\beta=0, \tag{10}$$

where $\Gamma^\mu_{\alpha\beta}$ are the Christoffel symbols. The equations for t and ϕ reduce to the quadratures (8) and (9). Using these equations and Eq. (1), we cast the equations for the remaining variables r and z in the convenient form

$$\ddot{r}=-\frac{1}{2f}[g^{tt}_{,r}E^2+g^{\phi\phi}_{,r}L_z^2+f_{,r}(\dot{r}^2-\dot{z}^2)+2f_{,z}\dot{r}\dot{z}], \tag{11}$$

$$\ddot{z}=-\frac{1}{2f}[g^{tt}_{,z}E^2+g^{\phi\phi}_{,z}L_z^2+f_{,z}(\dot{z}^2-\dot{r}^2)+2f_{,r}\dot{r}\dot{z}]. \tag{12}$$

To proceed further, it is convenient to define the prolate spheroidal coordinates u and v by

$$z = uv, \tag{13}$$

$$r^2 = (u^2-1)(1-v^2), \quad u \geqslant 1, \quad -1 \leqslant v \leqslant 1. \tag{14}$$

In these coordinates, Eq. (2) separates, and a general solution is obtained in a series of products of Legendre polynomials and zonal harmonics [14]. We must select a class of solutions that represents the physical system we are interested in: the field (1) should be the result of the superposition of a Schwarzschild black hole and multipolar contributions from an external halo. It is well known that in Weyl's coordinates the black hole's event horizon is represented as a singular bar lying on the symmetry axis, the inner region being excluded from the picture [13]; the ''bar'' singularity is therefore due to the choice of coordinates, which do not cover the whole space-time. On the other hand, the halo field, being the result of external matter sources, cannot have singularities in the region interior to the halo. The general solution that satisfies these conditions is

$$\psi = \tfrac{1}{2}\ln\left(\frac{u-1}{u+1}\right) + \sum_{n=1}^{\infty} a_n P_n(u) P_n(v). \tag{15}$$

The first term represents a Schwarzschild black hole with unit mass $m=1$, and the terms under the summation sign are multipolar contributions from the halo.

Using the coordinates u and v and the expression (15) for ψ, γ can be obtained from a straightforward integration of Eq. (3); the constant of integration is chosen so as to avoid conical singularities on the z axis, by imposing $\gamma = 0$ for $r = 0$ and $|z| > 1$.

In this article, we are interested in the multipole contributions only up to the octopole term [$n=3$ in Eq. (15)]. Redefining the coefficients in the expansion, we can write ψ as

$$\psi = \tfrac{1}{2}\ln\left(\frac{u-1}{u+1}\right) - Duv + (Q/6)(3u^2-1)(3v^2-1) + (O/10)uv(5u^2-3)(5v^2-3), \tag{16}$$

where D, Q, and O are related to the dipole, quadrupole, and octopole moments; we will refer to them as the dipole, quadrupole, and octopole strengths, respectively. Now an explicit expression for γ may be found by direct integration. Since the expressions are cumbersome and not particularly illuminating, we will not write them here; they can be found in [15–17]. We observe only that due to the nonlinearity of Einstein's equation, there are nonlinear terms of interaction between the multipole terms in γ: the gravitational field due to the different terms in the expansion (15) is not simply the superposition of the fields due to each term separately; this is a dramatic difference between the Newtonian and the relativistic theories.

We finish this discussion by recalling again that the coordinates u and v describe the metric only outside the black hole; in these coordinates, the event horizon is given by the segment $r=0, |z| \leqslant 1$. Since we are interested only in the motion of particles outside the event horizon, this singular behavior of the coordinates will not concern us here.

III. FRACTAL BASIN BOUNDARIES

We now review briefly some basic concepts on fractals in dynamical systems with escapes; a complete discussion is found in [1]. Systems allowing escapes have isolated unstable periodic orbits lying near the openings of the potential (we are considering Hamiltonian systems with two degrees of freedom, such as those treated here); these are the so-called Lyapunov orbits [2]. We define the *inner region* of the system to consist of the closed region in the configuration space bounded by the Lyapunov orbits and by the equipotential curves of a given energy. In order to simplify the discussion, we suppose for the moment that we have an inner region which has two distinct escapes, denoted by 1 and 2 (the generalization of the discussion for a higher number of escapes is straightforward). By *escape* we mean a route that allows the particle to leave the inner region permanently. The particular escape chosen by a particle is dependent on the initial conditions of that particle. For a given dynamical system and a given energy, the set of points in phase space that correspond to initial conditions such that the particle chooses escape 1 is the *basin* corresponding to escape 1; the basin corresponding to escape 2 is defined analogously. A point in phase space is defined to be a boundary point if every neighborhood of such a point contains points belonging to both basins. The basin boundary is the set formed by all the boundary points.

This system is chaotic if its basin boundary is fractal. Near a fractal basin boundary the points belonging to the different basins are mixed in a very complex way, down to arbitrarily small scales. If we draw a plot of the basins with a finite resolution, and amplify a region containing a fractal boundary, then no matter how much we amplify it, we will always find complex structures of intermixing points of both basins. This implies a strong dependency on the initial conditions near a fractal basin boundary.

If a system has a fractal basin boundary, then it has a fractal set of unstable ''eternal'' bounded orbits that never escape in the past and in the future (orbits that have never entered nor will ever leave the inner region), called the *chaotic saddle*. The basin boundary is formed by trajectories belonging to the stable manifold of the chaotic saddle, that is, by trajectories that never escape in the future (''trapped'' trajectories); the unstable manifold is formed by orbits that do not escape for $t \to -\infty$. The chaotic saddle, as well as its stable and unstable manifolds, are sets of zero measure within the phase space. The chaotic saddle is made by the infinite number of unstable periodic orbits (those that are not confined within KAM tori) and their homoclinic and heteroclinic crossings, which in the absence of KAM surfaces is the set of orbits that remain in the inner region for all times. It contains a countable infinity of periodic orbits and an uncountable infinity of aperiodic orbits. The chaotic saddle is part of the full *invariant set*, which is the set of *all* eternal orbits. Notice that in general not all eternal trajectories belong to the chaotic saddle: if the system has a stable periodic orbit for energies above the escape energy, then orbits near this one will also be eternal, and they form a nonzero-measure set of eternal orbits that are not part of the chaotic saddle. For Hamiltonian systems with two degrees of freedom such as the ones considered in this article, these orbits

are bounded by the outermost KAM torus, which separates the inner region filled with bounded orbits from the outer regions filled with escaping orbits (with the exception of the zero-measure set or orbits on the stable manifold of the chaotic saddle). The region of phase space bounded by the outermost KAM torus consists in general of a mixture of chaotic and regular orbits. This region is a nonhyperbolic part of the invariant set.

We note that, for a system (at a given energy) to have a fractal basin boundary, it not only needs to be nonintegrable, but also it must be such as to allow the presence of such a fractal set of trapped trajectories. In other words, the potential must be such that the particle can bounce back and forth many times before it escapes, if the system is to have a fractal basin boundary. The existence of such ''bouncing orbits'' is not a sufficient condition for a fractal boundary, but it is necessary. An example of a nonintegrable dynamical system with regular basin boundaries is given by the motion of null geodesics in the black hole plus dipole field, discussed in Sec. V.

The presence of a fractal set of unstable orbits is the result of transversal crossings of the stable and unstable manifolds of the Lyapunov orbits [2]. The basin boundaries between the different escapes are the stable manifolds of the Lyapunov orbits. The homoclinic and heteroclinic crossings imply a horseshoe symbolic dynamics, which is responsible for the chaos and the fractal character of the basin boundaries. The horseshoe dynamics results also in the existence of a set of countable unstable periodic orbits, which thus must exist if the system has a fractal basin boundary.

To give a quantitative measure of the sensitivity to initial conditions of a system with a fractal basin boundary, we define the box-counting dimension [18] of the boundary as follows: Let two points chosen randomically in a region of the phase space be separated by a small distance ϵ; it is then generally the case that the probability that the two points belong to different basins scales as

$$P(\epsilon)\propto\epsilon^{D-d}, \tag{17}$$

where D is the (integer) dimension of the region where the ensemble of points was chosen, and d is the (possibly noninteger) dimension of the intersection of the basin boundary with this region. If the boundary is nonfractal, then $d=D-1$, while if the boundary is fractal, we have $d>D-1$. By choosing randomly a large number of points in a region of the phase space for a certain fixed ϵ, we can calculate $P(\epsilon)$ numerically, and by doing this for several values of ϵ, we can calculate the fractal dimension d; this is the method we use in this article (see [18] for more details).

If our system has a stable periodic orbit for energies above escape, then as we said above it has a set of positive measure of nonescaping orbits bounded by tori in phase space. Escaping orbits that come close to this set stay in its neighborhood for a long time before leaving; in other words this set is ''sticky'' [7]. This complicates the task of calculating the box-counting dimension, for it demands a greater integration time. We also observe that for this same reason, the boundary between the escaping and the nonescaping regular orbits does not have a well-defined box-counting dimension.

We observe that since the fractal structure of the basin boundary is a topological feature of the dynamical system, it is a valid characterizations of chaos in general relativity.

IV. DYNAMICS OF MATERIAL PARTICLES

In this section, we study the motion of material test particles in the metric (16) for some choices of the multipole moments D, Q, and O. Important properties of the dynamics can be understood by means of the ''effective potential'' associated with this metric [19].

The boundary of the region in configuration space that is accessible to the particle is found by setting $\dot{r}=\dot{z}=0$ in Eq. (7), with $\delta=1$ for massive test particles:

$$E^2g^{tt}+L_z^2g^{\phi\phi}-1=0. \tag{18}$$

The ''effective potential'' $V(r,z)$ is then given by

$$V(r,z)\equiv E^2=\frac{1-L_z^2g^{\phi\phi}}{g^{tt}}. \tag{19}$$

Substituting for the Weyl metric (1), we have

$$V(r,z)=e^{2\psi}\left(1+\frac{e^{2\psi}L_z^2}{r^2}\right). \tag{20}$$

The region on the rz plane accessible to the particle is given by $V(r,z)\leqslant E^2$. Using Eq. (16) for ψ, we thus have an expression for the effective potential in terms of the multipole moments. We note that V depends only on ψ, and not on γ.

In the following subsections, we will analyze the dynamics for some interesting choices of D, Q, and O. For bounded trajectories, this system was shown through Poincaré sections to be chaotic [15–17].

A. Dipole potential

If we make $Q=O=0$ in Eq. (16), we have a pure dipole field together with a Schwarzschild black hole. The Newtonian system equivalent to this is the field due to a point mass superposed on a Newtonian shell dipole field, which is simply a field of constant acceleration. Bounded trajectories of the relativistic system have been studied, and chaos has been found using Poincaré sections [16]; the Newtonian system can be shown to be integrable, so the chaos is due to general relativistic contributions to the dynamics. We shall now study this system in the open regime, that is, with energies large enough to allow them to escape either to infinity or to the event horizon.

In Fig. 1 we show some contour levels of the effective potential $V(r,z)$ for $D=3\times10^{-4}$ and $Q=O=0$, with $L_z=3.0$. The first feature we notice is the ''tunnel'' formed by the equipotential curves for small values of r, which leads to the event horizon (remember that, in these coordinates, the event horizon is given by $r=0$ and $|z|\leqslant1$). This is the route followed by particles that fall into the black hole. We observe that V is invariant under the transformation $z\rightarrow-z$; $D\rightarrow-D$.

If a particle has high enough energy (E^2 higher than about 0.94 for the parameters of Fig. 1), it can also escape to in-

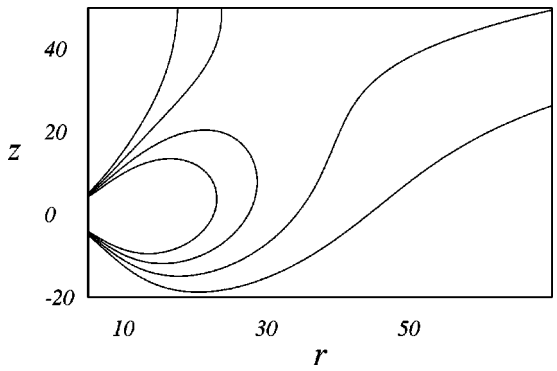

FIG. 1. Level contours of the effective potential for the dipole field ($Q=O=0$), with $D=3\times10^{-4}$ and $L_z=3.0$. The values of E^2 for the equipotentials are, from the inside out, 0.93, 0.94, 0.95, and 0.96. Since we have chosen units such that $G=c=m=1$ (m is the black hole's mass), all quantities in this and the other figures are dimensionless. In regular units, r and z are given in units of Gm/c^2, which is half the Schwarzschild radius of the black hole.

finity. This is shown clearly in Fig. 1 by the opening that appears in the equipotentials for high energies.

Now let us pick one specific value for the energy, for instance, $E^2=0.95$. At this energy, a particle's orbit can have three outcomes: (1) escape into the black hole; (2) escape to infinity; and (3) bouncing back and forth forever, and never leaving the inner region.

To investigate the nature of the basin boundaries, we need a portrait of the basins; to do this, we define a two-dimensional section of the three-dimensional energy shell of the phase space that is accessible to the particle. For $E^2=0.95$ we define this section as the set of initial conditions with spatial coordinates lying on the segment given by $z=0$ and $15\leqslant r\leqslant 25$, with velocities given by

$$\dot{r}=v\cos(\theta), \quad \dot{z}=v\sin(\theta), \tag{21}$$

where

$$v=(\dot{r}^2+\dot{z}^2)^{1/2}=\frac{1}{f}(1-E^2g^{tt}-L_z^2g^{\phi\phi}) \tag{22}$$

is defined by the conservation equation (7) with $\delta=1$, and $0\leqslant\theta\leqslant 2\pi$. This section is thus a topological segment of a cylinder embedded within the phase space, and we will denote it by S.

To obtain numerically the intersection of the basins with this section, we divide the intervals $15\leqslant r\leqslant 25$ and $0\leqslant\theta\leqslant 2\pi$ into 400 equal parts each; this defines a grid on S composed of 400×400 points. For each of these points, we integrate numerically the equations of motion for the dipole metric, and record the outcome: if the trajectory falls into the black hole (numerically, if r becomes too small, or less than 0.5 in this case), that initial condition belongs to basin 1; if the trajectory escapes to infinity (numerically, if r or z becomes too large, larger than 60 in this case), it belongs to basin 2; and if after a certain proper time τ_{max} (in this case we have chosen $\tau_{max}=100\,000$; for reference, the typical exit time is about 2000) the trajectory chooses none of the two escapes above, then we admit that it belongs to the set of ''trapped'' trajectories that never leaves the confining region.

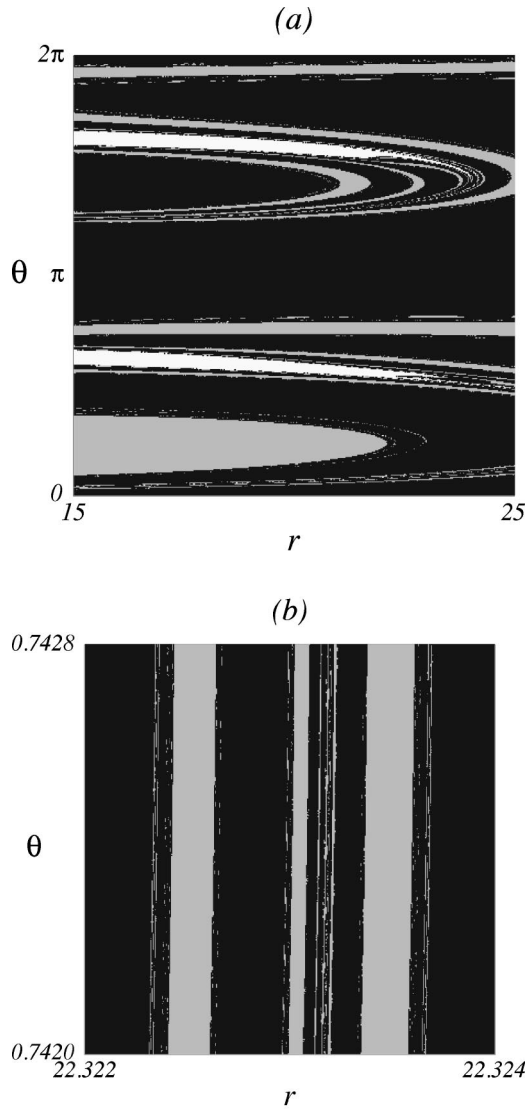

FIG. 2. Basin portrait of the section S of the phase space for the dipole field, with initial conditions on the axis $z=0$, for $D=3\times10^{-4}$, $L_z=3.0$, and $E^2=0.95$. The black areas correspond to regions of S whose trajectories fall into the event horizon; white areas correspond to trajectories that escape to infinity; and gray areas correspond to trajectories that remain trapped inside the confining region. This figure was calculated on a grid of 400×400 points. (b) is a magnification of (a).

We choose τ_{max} such that the set of ''trapped'' trajectories is well resolved for the scale of the grid we use.

The results of this calculation are shown in Fig. 2(a). A black dot means that the corresponding point (r,θ) in S belongs to basin 1; a white dot indicates that it belongs to basin 2; and a gray dot means it belongs to the set of ''trapped'' trajectories. We notice a complex Cantor-like mixing of basins, indicating that the structure continues down to smaller scales. This is confirmed by the amplification of a detail of Fig. 2(a) shown in Fig. 2(b). The area covered by Fig. 2(b) is about 10 orders of magnitude smaller than that of Fig. 2(a), giving strong evidence that the basin boundary is indeed fractal. We note that the set of trapped trajectories has a nonzero measure; this is clear from Fig. 2(a). Figure 3(a) shows the intersection of some of these trapped orbits with

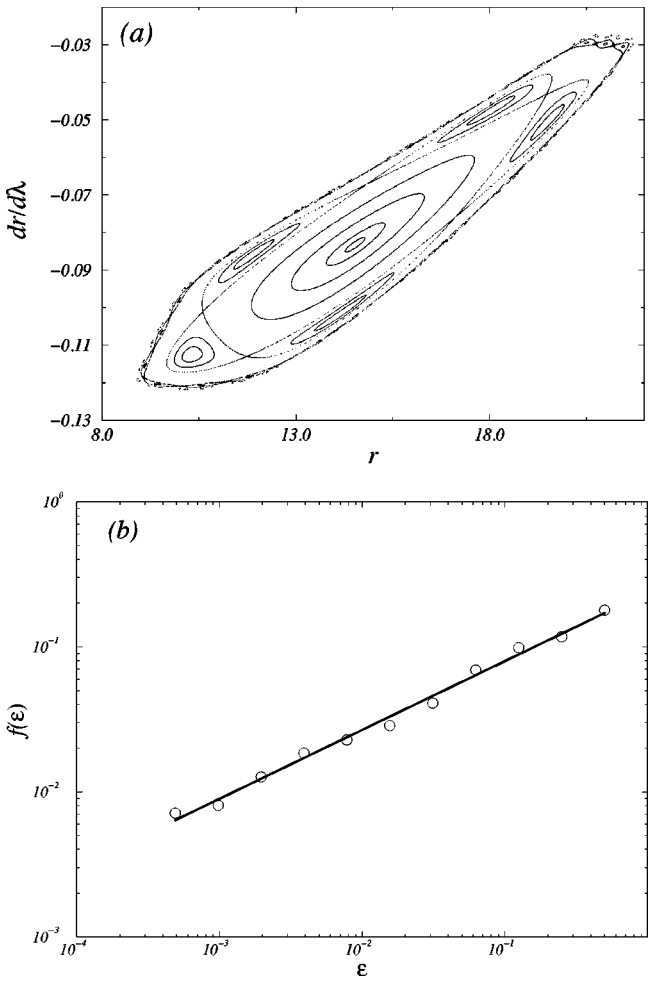

FIG. 3. (a) Poincaré section of trapped orbits, with the surface of section $z=0$, for $D=3\times10^{-4}$, $L_z=3.0$, and $E^2=0.95$; λ is an affine parameter. (b) Plot of the fraction of ''uncertain'' points $f(\epsilon)$ as a function of the separation ϵ.

the surface of section $z=0$. The parameters are the same as in Fig. 2.

To have a more precise and quantitative characterization of the fractal structure seen in Fig. 2, we proceed to the calculation of the fractal dimension, as discussed in Sec. III. The random points are chosen in S, and for each point (r,θ) we find through numerical integration to which of the basins it belongs, and then do the same for two nearby phase-space points given by $r+\epsilon$ and $r-\epsilon$ and the same θ. If all three points do not belong to the same basin, then the point (r,θ) is considered an ''uncertain'' point, meaning that it lies close to a basin boundary. For a large number N of points randomly chosen in S, the fraction of uncertain points is $f(\epsilon)=N'/N$, where N' is the number of uncertain points found in the sample of N points. For N large enough, f is proportional to P in Eq. (17); finding in this way f for several values of ϵ, a log-log plot of $f(\epsilon)$ should give a straight line, and the basin boundary dimension d is found by the angular coefficient through Eq. (17). For reasons explained in Sec. III, we calculate d by choosing points in a region that does not intersect the trapped region bounded by KAM tori. By getting rid in this way of the ''stickiness'' of the regular region, we are able to obtain a meaningful result for d.

The results are shown in Fig. 3(b). We have chosen N such that $N'>100$; this means a statistical uncertainty of about 10% in f. We see that the points lie on a clearly defined straight line; the angular coefficient is $\alpha=0.47\pm0.02$, which gives a dimension of $d=1.53\pm0.02$, showing unambiguously that the boundary is fractal. We remember that d is the dimension of the intersection of the basin boundary with the two-dimensional section S; the dimension of the basin boundary in the accessible three-dimensional space is $d+1$. We have calculated d for some subregions of S, and we have always obtained the same value to within the statistical uncertainty, showing that the method is self-consistent and the result is meaningful.

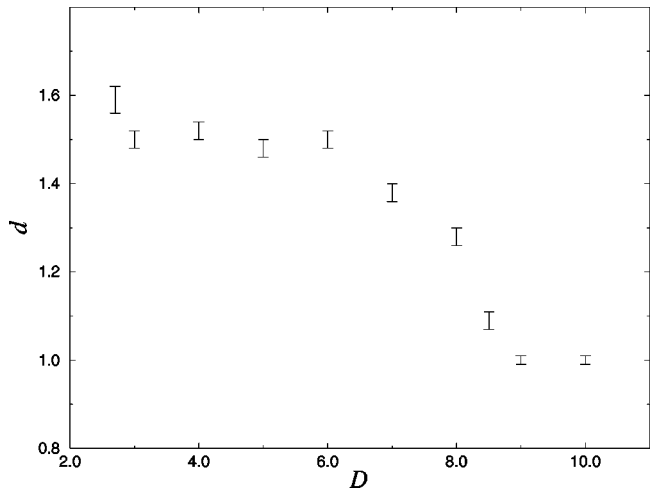

FIG. 4. Box-counting dimension of the basin boundary as a function of the dipole strength D, for $E=0.95$ and $L_z=3.0$.

We have studied how the box-counting dimension changes as we change the various parameters of the metric. If $D=0$, a particle needs an energy E higher than 1 to be able to escape to infinity. If $D\neq0$, the escape energy becomes less than 1, and depends on the angular momentum L_z. We denote the escape energy by $E_0=E_0(L_z)$. The basin boundary dimension d is defined only for $E>E_0$. We have found that for $E>1$, $d=1$ (to within the statistical error), and the basin boundary is regular. We have verified this result for several values of L_z and E, and three different values of D.

We have also investigated how d changes with the dipole strength D. In the limit $|D|\to\infty$, we have a field dominated by the dipole component; the geodesics defined by a pure dipole field are integrable, and thus we expect d to approach 1 for high values of D. If we decrease D enough, we end up reaching a value D_0 below which the particle can no longer escape to infinity, and d is no longer well defined. Near $D=D_0$, with $D>D_0$, the opening of the equipotential to the escape to infinity is small, and the particle is likely to bounce more times before it escapes through this route than in the case of higher values of D, and we accordingly expect the chaos to be ''larger'' in this case, that is, d to be larger. These features are indeed verified in a plotting of d versus D for $E^2=0.95$ and $L_z=3.0$, shown in Fig. 4. For these values of D and L_z, we have $D_0\equiv2.5\times10^{-4}$. The system is regular $(d=1\pm0.01)$ for $D\geqslant9\times10^{-4}$, and d reaches its highest value of about 1.6 at $D=D_0$.

B. Quadrupole potential

We next turn to the case $D=O=0$. This quadrupole field has a reflection symmetry with respect to the z axis: the

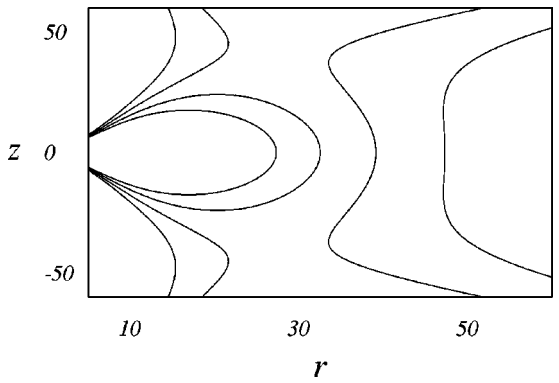

FIG. 5. Level contours of the effective potential for a quadrupole field ($D=O=0$) with a prolate halo ($Q=-4\times10^{-6}$) and $L_z=2.6$. The values of E^2 for the equipotentials are, from the inside out, 0.93, 0.94, 0.95, and 0.96.

metric is unchanged by $z\rightarrow -z$. For the oblate case ($Q>0$), the open equipotentials are similar to the pure dipole case discussed above (except for the aforementioned symmetry). A more interesting choice is $Q<0$ (prolate case); in this case, as shown in Fig. 5, there are two different escapes to infinity, besides the escape into the event horizon. We investigate this system for the energy $E^2=0.97$, with $L_z=2.6$ and $Q=-4\times10^{-6}$. For these parameters, the invariant set appears to have zero measure, since we were not able to find any stable orbit in the inner region.

We proceed as we did for the dipole case. We choose initial conditions in the segment $r=25.0$, $|z|<25.0$; the velocities are given by Eq. (21). The results are in Fig. 6(a), with black dots denoting trajectories that escape upward, white dots denoting trajectories that escape downward, and gray dots denoting trajectories that fall into the event horizon. Figure 6(b) shows an amplification of a very small area of Fig. 6(a), and the absence of smoothness in the basin boundary shows clearly its fractal character. The fractal dimension was computed as described above, and the value we obtained was $d=1.60\pm0.03$. In the corresponding oblate case, with $Q=+4\times10^{-6}$ and all other parameters being equal, we found no detectable chaos, and the basin boundary was found to be regular, with $d=1$ to within our numerical accuracy. This is in agreement with the results found in [17], where it was found (by using Poincaré sections) that for a black hole plus oblate quadrupole field the bounded orbits show an almost regular behavior, the chaotic regions being restricted to very small volumes in phase space, while the corresponding prolate field shows strong chaos.

We have calculated d for other values of the energy and angular momentum, and we found that, as opposed to the dipolar halo system studied in the previous section, this system is chaotic for $E>1$. In fact, we found that the boundary is fractal for arbitrarily large values of the energy (for $Q<0$), as far as we have been able to investigate; this appears to be an important difference between the dipolar and quadrupolar halos.

Since the basin boundary between the escapes is the stable manifold of the chaotic saddle, we have associated with the chaos in the choice of the escape route a chaos in the escape time as well, as is well known in chaotic scattering. This happens because orbits starting from very close

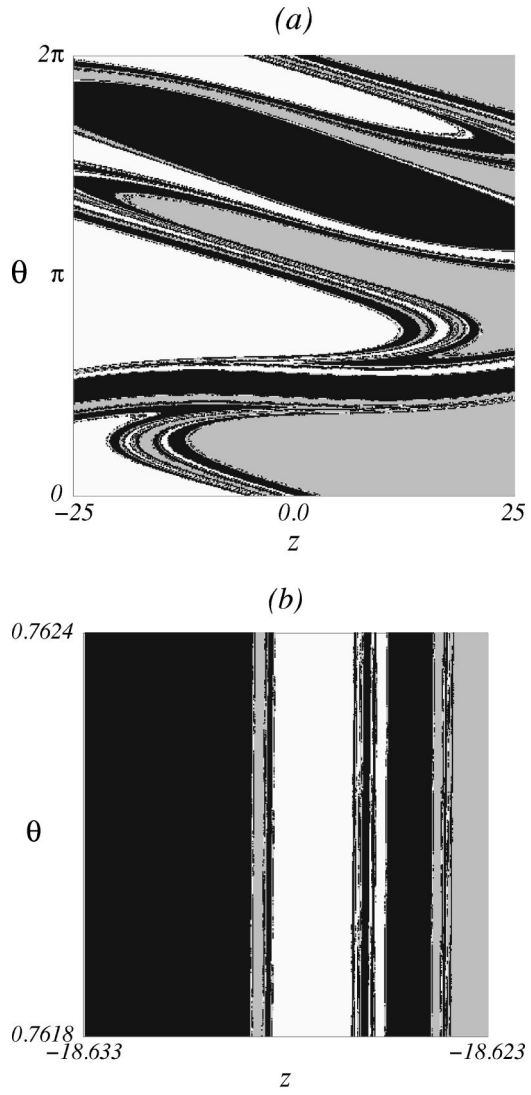

FIG. 6. Basin portrait for the quadrupole field, with $Q=-4\times10^{-6}$ and $L_z=2.6$. Black areas denote regions whose trajectories fall into the event horizon; gray areas correspond to trajectories that escape toward $z\rightarrow+\infty$; and white areas correspond to trajectories that escape toward $z\rightarrow-\infty$. (b) is a magnification of (a).

initial conditions may make a different number of bounces before escaping, leading to very different escape (proper) times. We have illustrated this by finding numerically the escape proper times τ_e for orbits starting from a fixed position $r=25$, $z=0$, for several velocity angles θ, as defined by Eq. (21). We plot $\tau_e(\theta)$ in Fig. 7(a). The ''spiked'' character of the graph is striking, suggesting a fractal structure. This is confirmed by Fig. 7(b), which shows that the function $\tau_e(\theta)$ has a fractal set of singular points, where $\tau_e(\theta)$ goes to infinity; this set is the intersection of the line of initial conditions with the basin boundary. We observe that the escape time τ_e is to some extent arbitrary, because it depends on where we stop the integrations of the trajectories before we consider them to have escaped. However, the fractal structure seen in Fig. 7 is topological, and is not affected by this choice. These features of the escape time function remain the same for r and z within the inner region.

In order to gain more insight into the fractal structure of the basin boundary and its related complex dynamics, we

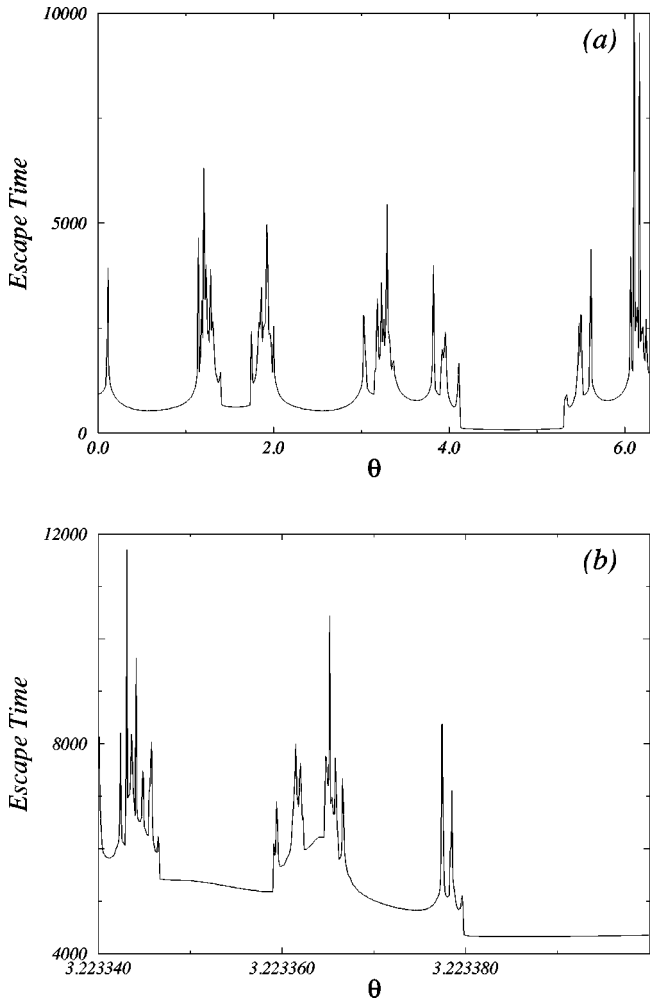

FIG. 7. Time of escape versus the velocity angle ($Q=-4\times10^{-6}, L_z=2.6$), for $r=25$ and $z=0$. (b) is a magnification of (a).

now define a surface of section in phase space denoted by $\mathcal{P}$ and given by $\dot{z}=0$, for a given E and L_z. We define I_n($n\geqslant 1$) as the set of points on the surface of initial conditions S that generate orbits that cross $\mathcal{P}$ at least n times in the negative direction (that is, satisfying $\ddot{z}<0$) before escaping. Obviously I_n is a subset of I_k if $k<n$, and we have that

$$I_1 \supset I_2 \supset I_3 \supset \cdots. \tag{23}$$

For systems without KAM tori (as appears to be the case of the quadrupole field with the parameters of Fig. 7), the basin boundary is given by $\lim_{n\to+\infty} I_n$. If we let I_n, with n being a negative integer, denote the set of points in S corresponding to past-directed orbits that cross $\mathcal{P}$ in the negative direction at least $|n|$ times, then the unstable manifold of the chaotic saddle is analogously given by $\lim_{n\to-\infty} I_n$. Defining now the set $R_n = I_n \cap I_{-n}$, the chaotic saddle is given by $\lim_{n\to+\infty} R_n$. This simply states that the chaotic saddle is the intersection of its stable and unstable manifolds.

The mechanism of the construction of the fractal basin boundary by the dynamics of the system may be followed by examining the sets $I_n(n>0)$. Figures 8(a), 8(b), and 8(c) show I_1, I_2, and I_3, respectively, using the same grid as that of Fig. 7(a). As n increases, the structure of I_n becomes more and more complicated: every step $I_n \to I_{n+1}$ results in taking from I_n increasing numbers of ever thinner strips, alternately. We recognize this as the mechanism for the construction of a Cantor set, in the limit $n\to+\infty$.

We can follow in the same way the construction of the chaotic saddle itself: in Fig. 8(d) we show R_2; compare this with Fig. 8(b).

The Newtonian system equivalent to the multipole field we are dealing with is given by the Hamiltonian

$$H=\tfrac{1}{2}(p_r^2+p_z^2)+V(r,z), \tag{24}$$

where $V(r,z)$ is the effective potential

$$V(r,z)=\frac{L_z^2}{2r^2}-\frac{1}{r}+\psi(r,z), \tag{25}$$

and ψ is given by Eq. (16). For the dipole field ($Q=O=0$), as we mentioned before, the Hamiltonian (24) is integrable. For the quadrupole field, however, it is not [15], so we expect to have a fractal basin boundary for this case as well. Figure 9 shows some level contours of V with $L_z=2.6$ and $Q=-4\times10^{-6}$, $D=O=0$; these are the same parameters we have used for the relativistic case. For this negative value of Q, we have two escapes (for $Q>0$, there is only one escape). Since we want to compare the Newtonian and the relativistic cases, we choose the energy to be $E-1$, where E is the energy we used in the relativistic case, which gives -0.0151. We proceed as in the relativistic case to calculate the basin boundary dimension. The initial conditions are chosen in the segment $|z|<5$, $r=13$. The result is $d=1.64\pm0.02$, which is roughly the same value (actually a little larger) we obtained for the relativistic case.

C. Quadrupole + octopole potential

The last case we investigate in this section is the field formed by the superposition of the quadrupole and octopole components, $D=0$ with Q, $O\neq0$. The octopole term breaks the reflection symmetry of the quadrupole potential, as can be seen in Fig. 10, which shows some level contours of the effective potential for $D=0$, $Q=-4\times10^{-6}$, $O=-1\times10^{-7}$, and $L_z=2.6$. We still have three escapes as in the previous case, but the equipotentials are distorted, and are no longer symmetrical with respect to the $z=0$ axis. We select the energy $E^2=0.97$, and pick the initial conditions on the segment $|z|<20$, $r=20$. Using these parameters, we have calculated the basin boundary dimension, and found $d=1.59\pm0.02$, which is practically the same value obtained for the pure quadrupole field $O=0$. If we calculate d for the pure octopole field $O=-10^{-7}$, $Q=0$, keeping the other parameters fixed, we find $d=1.70\pm0.02$, which is *larger* than the value obtained for the mixed field. This is a somewhat surprising result, and it shows that a ''more complicated'' field does not necessarily result in a more complicated (or ''more chaotic'') motion.

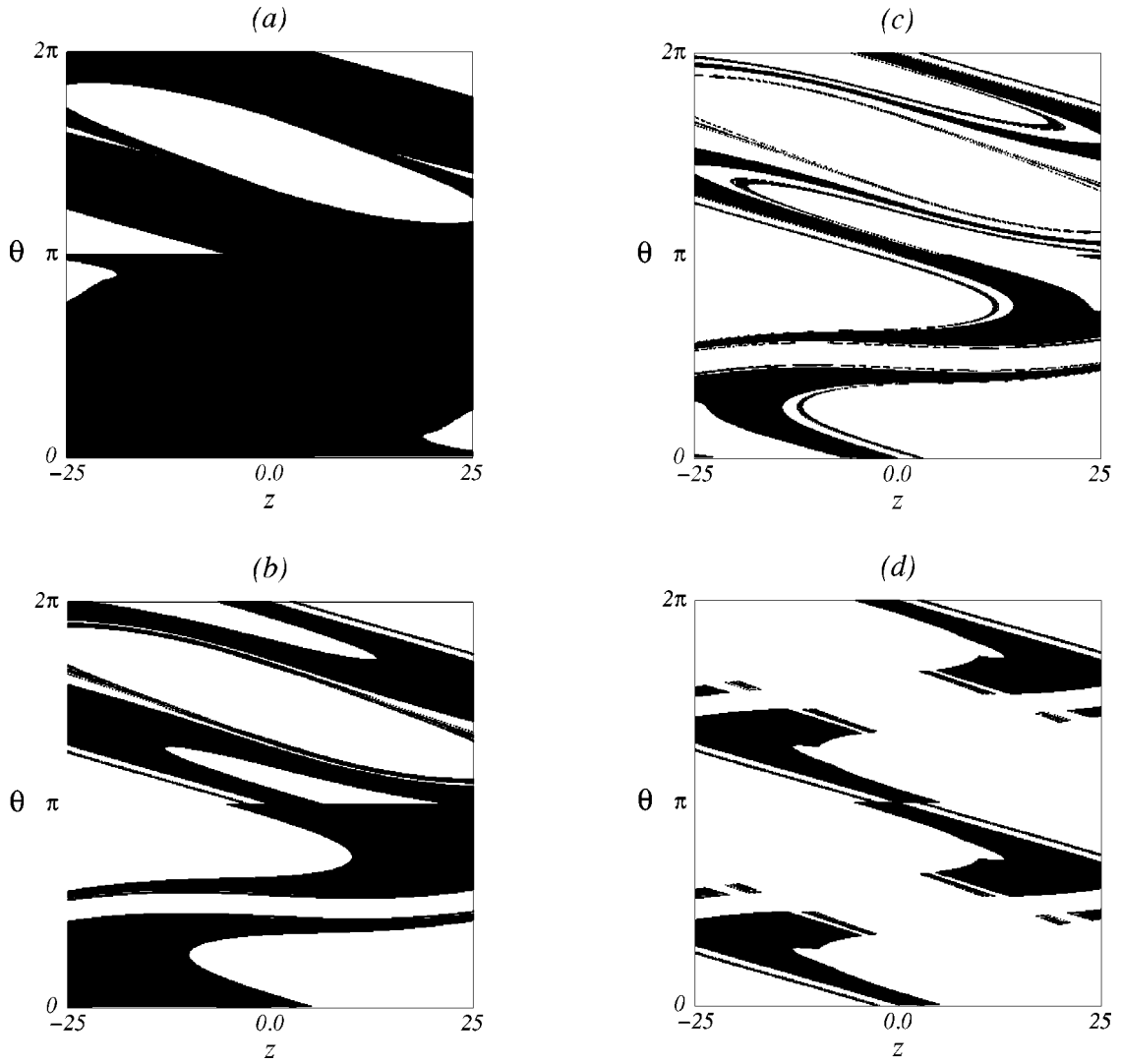

FIG. 8. (a) I_1, (b) I_2, (c) I_3, (d) R_2, for $Q=-4\times10^{-6}$, $L_z=2.6$, and $D=O=0$.

V. THE NULL GEODESICS

We will now study the dynamics of the null geodesics in the metric (16). For null geodesics, $ds^2=0$ and $\delta=0$ in Eq. (7), and we have

$$E^2 g^{tt}+L_z^2 g^{\phi\phi}+f(\dot{r}^2+\dot{z}^2)=0, \tag{26}$$

with $f=-g_{zz}=-g_{rr}$. The effective potential is then given by

$$\frac{E^2}{L_z^2}\equiv\frac{1}{b^2}=V(r,z)=-\frac{g^{\phi\phi}}{g^{tt}}=\frac{e^{4\psi}}{r^2}, \tag{27}$$

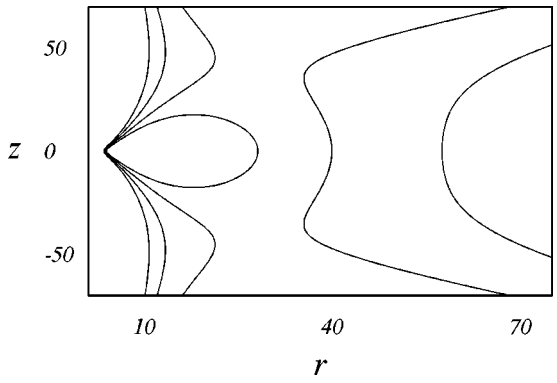

FIG. 9. Level contours of the effective potential for the classical quadrupole field with $Q=-4\times10^{-6}$ and $L_z=2.6$. The values of E^2 for the equipotentials are, from the inside out, 0, -0.01, -0.02, and -0.03.

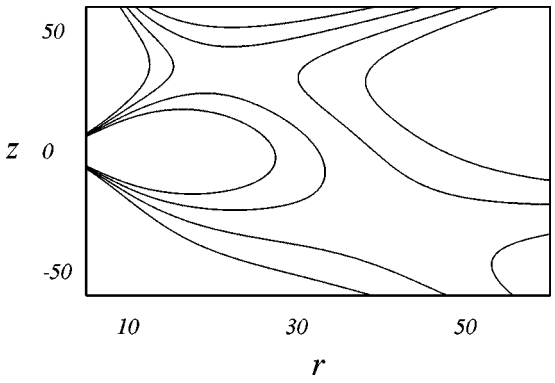

FIG. 10. Level contours of the effective potential for the field with $D=0$, $Q=-4\times10^{-6}$, $O=-10^{-7}$, and $L_z=2.6$. The values of E^2 for the equipotentials are, from the inside out, 0.94, 0.95, 0.96, and 0.97.

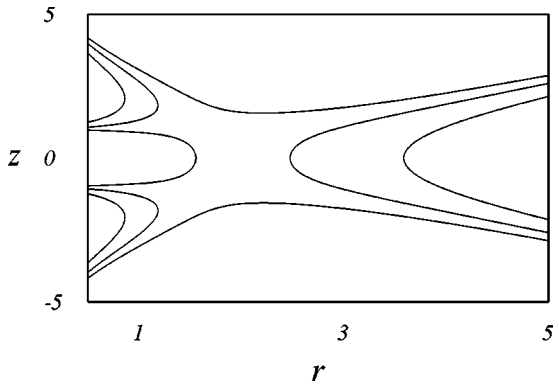

FIG. 11. Level contours of the effective potential for null geodesics for the quadrupole field $Q=-0.05$, $D=O=0$. The values of b^2 (b is the impact parameter with respect to the symmetry axis) are, from the inside out, 10.0, 15.0, and 20.0.

where b is the impact parameter with respect to the z axis. The curve $V(r,z)=1/b^2=\text{const}$ is the boundary of the regions of the rz plane accessible to a particle having an impact parameter of b. We notice that in the case of massive particles, the effective potential depends separately on E and L_z, while for the case of massless particles, it depends only on the ratio $E/L_z=b$. The equations of motion for the null geodesics are Eqs. (11) and (12), together with the quadratures (8) and (9), with E and L_z related by $b=L_z/E$. The initial conditions must be such as to satisfy the constraint (26).

In the case of the dipole field ($Q=O=0$), we find that below a certain value of the impact parameter b the equipotential curves open, and the orbits can either fall into the event horizon or escape to infinity. We find, however, by numerical calculations of pictures of the basins, which show regular basin boundaries, and by the computation of the basin boundary dimension, which gives $d=1$ to within the statistical uncertainty, that the basin boundaries are regular and the system presents no chaos. This result holds for all values of D and b we have investigated, and it seems safe to conclude that massless test particles in the field of a black hole surrounded by a dipolar material halo move in regular orbits.

When we introduce terms of higher order in the multipolar expansion of the halo, this situation changes. We illustrate this with a pure quadrupolar halo. If $Q>0$, there are only two escapes (toward infinity and toward the event horizon), and the orbits are again regular. If $Q<0$, however, we have three escape routes (toward the event horizon, toward $z\to\infty$, and toward $z\to-\infty$), and chaotic behavior arises. This can be seen in Fig. 11, where we show some equipotential curves for $Q=-0.05$, with $D=O=0$. Choosing $b^2=12.5$, we obtain a picture of the basins by numerical integration, with the initial conditions in the segment $r=2,|z|<2$. The result is shown in Fig. 12(a), and an amplification of several orders of magnitude [Fig. 12(b)] shows that the basin boundary is fractal. This is further confirmed by the calculation of the basin boundary box-counting dimension, which yields $d=1.25\pm0.02$. We have verified that an octopole halo also gives rise to chaos, as is probably the case for multipole terms of higher order.

Now we make some general remarks on the motion of

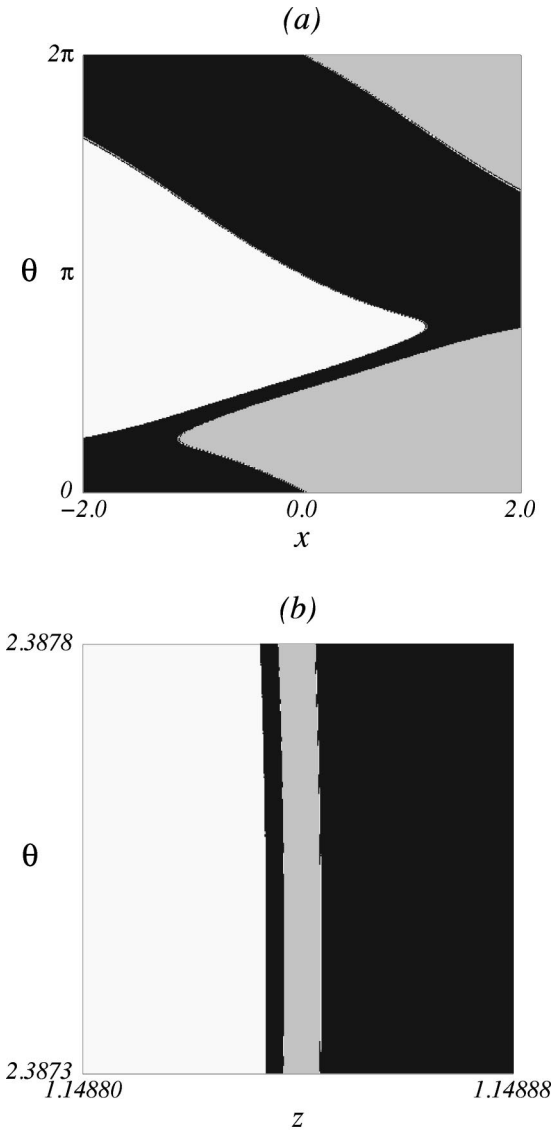

FIG. 12. Basin portrait for null geodesics with $Q=-0.05$, $D=O=0$, and $b^2=12.5$. Areas in black correspond to trajectories that fall into the event horizon; areas in gray correspond to trajectories that escape toward $z\to+\infty$, and areas in white denote trajectories that escape to $z\to-\infty$.

massless particles in the metric (16). The absence of stable periodic orbits, and therefore of a nonzero-measure set of confined orbits, was verified in all cases we have investigated, leading us to make the hypothesis that this is a general feature of the motion of zero mass particles in the black-hole–halo field; we speculate that this may be the case for all static axisymmetric metrics. We also observed that, in all cases in which there are only two escapes (as, for instance, in the dipolar halo field and in the quadrupolar field with $Q>0$), the motion of zero rest mass particles is always regular, as opposed to the motion of material particles in the same fields. When there are three or more escapes, on the other hand, chaotic behavior appears. We have found, however, that the motion of massless particles is always less chaotic (that is, the box-counting dimension d of the basin boundary is lower) than the motion of massive particles for the same field, for all cases considered by us.

VI. CONCLUSIONS

In this article we have considered core-shell gravitational models, which could describe inner regions of elliptical galaxies. Our study focused on the dynamics of test particles moving in the gravitational field of such objects, and we have particularly studied unbounded motions and their associated escape dynamics, both for massive test particles and for light.

In the case of massive particles, chaos was found in the form of fractal basin boundaries. We single out the case of a dipolar halo, which has a Newtonian counterpart that is known to be integrable; the chaos for this case is thus a result of relativistic corrections to the dynamics. This is compatible with earlier results obtained with bounded orbits [15]. Also for this case, we have investigated the set of trapped orbits with nonzero measure, and we showed that it is formed by orbits that are bound by KAM tori in phase space. This means that even for energies above the escape energy, there are regions in phase space wherein the motion remains bounded. Such stable regions are surrounded by unstable ones, where particles either fall into the black hole or escape to infinity, these two outcomes being separated in phase space by a fractal basin boundary.

We have found that the core-dipole system is not chaotic for energies above 1, which is the escape energy for an isolated nonrotating black hole. The system appears to be most chaotic (its boundary dimension attains its highest value) for energies near escape.

If the halo is composed of a pure quadrupole term, the situation changes. For a prolate halo ($Q<0$), there can be three escape routes, as opposed to only two present in the dipole case, and in this case the system is chaotic for arbitrarily large values of the energy, as far as we could determine. Oblate halos ($Q>0$) show no detectable chaos for the parameters we have used, as opposed to the prolate ones. This is in agreement with results found previously for bounded orbits [17], which show that oblate halos have very little chaos.

In the case of massless particles (null geodesics), we find that the black hole + dipolar halo system is not chaotic, the basin boundary between the escapes being regular for all values of the parameters we have investigated. If we add a quadrupole term to the halo, the motion becomes chaotic if $Q<0$; the orbits are still regular for $Q>0$, further confirming that oblate halos are a weak source of chaos. Terms of higher order also introduce chaos in the system. In contrast to the case of material particles, we have not found any stable periodic orbit, with its accompanying nonzero-measure set of confined orbits. We believe the absence of stable periodic orbits of massless particles is a general feature of axisymmetric static gravitational fields.

ACKNOWLEDGMENT

This research was partially funded by FAPESP and CNPq.

[1] E. Ott, *Chaos in Dynamical Systems* (Cambridge University Press, Cambridge, 1993).
[2] G. Contopoulos, Astron. Astrophys. **231**, 41 (1990).
[3] G. Contopoulos, H.E. Kandrup, and D. Kaufmann, Physica D **64**, 310 (1993).
[4] S. Bleher, C. Grebogi, E. Ott, and R. Brown, Phys. Rev. A **38**, 930 (1988).
[5] J.M.T. Thompson, Proc. R. Soc. London, Ser. A **421**, 195 (1988).
[6] H.B. Stewart, J.M.T. Thompson, Y. Ueda, and A.N. Lansbury, Physica D **85**, 259 (1995).
[7] F. Christiansen and P. Grassberger, Phys. Lett. A **181**, 47 (1993).
[8] *Deterministic Chaos in General Relativity*, edited by D. Hobill, A. Burd, and A. Coley (Plenum Press, New York, 1994).
[9] N.J. Cornish and J.J. Levin, Phys. Rev. D **53**, 3022 (1996).
[10] G. Contopoulos, Proc. R. Soc. London, Ser. A **431**, 183 (1990).
[11] G. Contopoulos, Proc. R. Soc. London, Ser. A **435**, 551 (1991).
[12] C.P. Dettmann, N.E. Frankel, and N.J. Cornish, Fractals **3**, 161 (1995).
[13] D. Kramer, H. Stephani, and E. Herlt, *Exact Solutions of Einstein's Field Equations* (Cambridge University Press, Cambridge, 1980).
[14] A.G. Webster, *Partial Differential Equations of Mathematical Physics* (Dover Publications, New York, 1966).
[15] W.M. Vieira and P.S. Letelier, Phys. Rev. Lett. **76**, 1409 (1996).
[16] W.M. Vieira and P.S. Letelier, Phys. Lett. A **228**, 22 (1997).
[17] W.M. Vieira and P.S. Letelier, Astrophys. J. **513**, 383 (1999).
[18] C. Grebogi, S.W. McDonald, E. Ott, and J.A. Yorke, Phys. Lett. **99A**, 415 (1983).
[19] C.W. Misner, K.S. Thorne, and J.A. Wheeler, *Gravitation* (W.H. Freeman and Company, New York, 1973).